Title
Hydroisomerization of n -hexadecane: remarkable selectivity of mesoporous silica post-synthetically modified with aluminum

Journal
Catalysis Science & Technology, 7(8)

ISSN
2044-4753

Authors
Sabyrov, Kairat
Musselwhite, Nathan
Melaet, Gérôme
et al.

Publication Date
2017

DOI
10.1039/c7cy00203c

Peer reviewed

Hydroisomerization of n-Hexadecane: Remarkable Selectivity of Mesoporous Silica Post-Synthetically Modified with Aluminum

Kairat Sabyrov,[a,c] Nathan Musselwhite,[a,c] Gérôme Melaet,[b] and Gabor A. Somorjai[a,b,c]*

[a]*Chemical Sciences Division, Lawrence Berkeley National Laboratory, 1 Cyclotron Road, Berkeley, California 94720, United States.*

[b]*Materials Sciences Division, Lawrence Berkeley National Laboratory, 1 Cyclotron Road, Berkeley, California 94720, United States.*

[c]*Department of Chemistry, University of California at Berkeley, Berkeley, California 94720, United States.*

KEYWORDS: Platinum nanoparticles, mesoporous silica, n-hexadecane, hydroisomerization, mesoporous zeolite, bifunctional catalyst

ABSTRACT: As the impact of acids on catalytically driven chemical transformations is tremendous, fundamental understanding of catalytically relevant factors is essential for the design of more efficient solid acid catalysts. In this work, we employed post-synthetic doping method to synthesize highly selective hydroisomerization catalyst and to demonstrate the effect of acid strength and density, catalyst microstructure, and platinum nanoparticle size on reaction rate and selectivity. Aluminum doped mesoporous silica catalyzed gas-phase n-hexadecane isomerization with remarkably high selectivity, producing substantially higher amount of isomers than traditional zeolite catalysts. The main reason for its high selectivity was found to be mild acidic sites generated by post-synthetic aluminum grafting. The flexibility of post-synthetic doping method enabled us to systematically explore the effect of acid site density on reaction rate and selectivity, which has been extremely difficult to achieve with zeolite catalysts. We found that higher density of Brønsted acid sites leads to higher cracking of n-hexadecane presumably due to increased surface residence time. Furthermore, regardless of pore size and microstructure, hydroisomerization turnover frequency linearly increased as a function of Brønsted acid site density. In addition to strength and density of acid sites, platinum nanoparticle size affected catalytic activity and selectivity. Smallest platinum nanoparticles produced the most effective bifunctional catalyst presumably because of higher percolation into aluminum doped mesoporous silica, generating more 'intimate' metallic and acidic sites. Finally, aluminum doped

silica catalyst was shown to retain its remarkable selectivity towards isomers even at increased reaction conversions.

INTRODUCTION

Branched alkanes are more desirable than their linear counterparts due to better performance of the former as a motor fuel and lubricant oil.[1-5] In the modern petroleum industry, hydroisomerization of long-chain linear alkanes has become a key process for increasing the quality of hydrocarbons.[1, 3] High value or high octane gasoline is obtained via the skeletal isomerization of linear alkanes contained in the naphtha feedstock,[6-9] whereas lubricant oil with high viscosity index and low-pour-point properties is synthesized via catalytic isomerization of heavy-gas oil.[3, 10, 11] The most common undesired process for hydroisomerization is cracking, i.e., the conversion of the reactant molecule into shorter chain hydrocarbons.[9, 12] The cracking process also forms higher amount of carbonaceous deposits or coke on catalyst surface, which can deactivate the catalyst more rapidly.[12, 13]

In the catalytic reforming of heavy-gas feedstocks of crude oil, long-chain linear alkanes are isomerized using bifunctional catalysts, which typically contain both hydrogenation/dehydrogenation sites and acidic sites. Commonly used bifunctional catalysts are platinum or palladium containing solid acids such as zeolites, aluminas or aluminosilicates, and silicoaluminophosphates.[9, 14-16] Numerous solid acids and their combinations with noble metals have been studied to understand reaction mechanism and improve the efficiency of the processes.[13, 17] Generally, catalysts with a lower degree of acidity and a high hydrogenation activity are favorable for maximizing hydroisomerization turnover rate, since catalysts containing milder acidic sites can limit cracking.[16, 18] Furthermore, the degree of noble metal dispersion, interplay between hydrogenation/dehydrogenation and acidic sites, and spatial constraints within zeolitic micropores were demonstrated to affect isomerization activity and selectivity.[16, 19-21]

Even though hydroisomerization process has been extensively studied for decades, there is a need for highly selective catalyst, especially at high temperature conditions. In industrial hydrocarbon conversion settings, high temperature conditions are favored to increase the overall

turnover rate of the reactions. However, the cracking tendency of the most aluminosilicate catalysts, such as zeolites, increases with increasing reaction temperature due to their strong acidity. In addition, achieving high isomerization selectivity for longer chain alkanes becomes more difficult at higher reaction temperatures as hydrocracking and hydrogenolysis start to compete with the isomerization. In this work, hydroisomerization of n-hexadecane was used as a model reaction to demonstrate that mesoporous silica post-synthetically modified with aluminum can catalyze the reaction with exceptionally high selectivity, reaching ~100%. The remarkable selectivity of the catalyst facilitated much higher isomerization yield as compared to mesporous zeolites with BEA and MFI microstructures. Superior catalytic performance of the aluminum modified silica catalyst is primarily due to its milder acidic character produced by post-synthetic modification of the silica surface.[16] Furthermore, post-synthetic doping method allowed us to systematically explore the effect of acid density, catalyst microstructure, and platinum nanoparticle size on reaction rate and selectivity. In zeolite catalysis, detailed characterization of these factors has been extremely difficult because the structure of traditional zeolites is rather rigid and the attempts to change the zeolitic framework concomitantly change its microstructure, acid site strength and distribution, and crystallinity. The studies on aluminum doped mesoporous silica showed that hydroisomerization turnover frequency linearly increases as a function of surface Brønsted acid site density. In addition to producing the highest amount of isomers, the catalyst with increased density of acid sites considerably cracked n-hexadecane presumably due to increased residence time of surface intermediate species. Furthermore, smallest platinum nanoparticles supported on aluminum modified mesoporous silica formed the most active, selective, and stable catalyst. The dependence of reaction rate and selectivity on platinum nanoparticle size was discussed in light of nanoparticle percolation and intimacy criterion. Finally, the highly selective silica catalyst was tested at increased reaction conversions. Unlike at high reaction temperatures, the catalyst retained its high selectivity at relatively high conversions achieved with increased catalyst mass loading.

EXPERIMENTAL SECTION

Synthesis

Platinum nanoparticles with well-defined particle size, mesoporous and microporous SiO_2, and mesoporous zeolites with BEA and MFI framework types were synthesized according

to the methods published previously.[16, 22, 23] The details of the synthesis and post-synthetic doping of the silica with aluminum can be found in the electronic supporting information (ESI). Polyvinylpyrrolidone (PVP) capped platinum nanoparticles were dispersed on aluminum modified mesoporous silica and zeolite catalysts by mixing ethanolic suspensions of the support material and platinum nanoparticles. 10 mL of the final suspension (1 mg/ml platinum nanoparticles and 50 mg/ml support material) was then sonicated using a commercial ultrasonic cleaner (Branson, 1510R-MT, 70 W, 42 kHz) for ~30 minutes at room temperature to give ~0.5% platinum by weight. The loaded catalysts then were centrifuged and washed 3 times with ethanol and dried in oven at 80 ºC. The catalysts were indicated as Pt/Al-MCF-17, Pt/BEA, Pt/MFI, Pt/Al-SBA-15 and Pt/Al-SPP for platinum nanoparticles supported on aluminum modified mesostructured cellular foam, mesoporous BEA and MFI zeolites, aluminum modified Santa Barbara amorphous and aluminum modified self-pillared pentasil, respectively. Before catalytic reaction studies, the catalysts were treated at 360 ºC for 2 hours under reducing atmosphere (H_2 = 10 sccm, N_2 = 10 sccm) to ensure that the organic stabilizer (PVP) is removed and the platinum nanoparticles are completely reduced to metallic state. Our previous work demonstrated that these treatment conditions are sufficient to significantly decompose the capping agent without inducing detectable changes in nanoparticle size or shape.[24]

Characterization

The catalysts were characterized before and after the reaction by transmission electron microscope (TEM, 200 kV, Hitachi) for the characterization of morphology, microstructure and size of the platinum nanoparticles and silica samples. Aqueous suspensions of the catalysts were prepared and a small drop of the diluted suspension was dried on a TEM copper grid coated with a carbon film (200 mesh grid, SPI supplies). The total specific surface area of the catalysts was determined via N_2 (UHP grade, 99.999%, PraxAir) physisorption at 77 K using an Autosorb-1 (Quantachrome) analyzer. The platinum and aluminum amounts were determined by inductively coupled plasma atomic emission spectroscopy (ICP-AES) using a Perkin Elmer optical emission spectrometer (Optima 7000 DV). The concentration and strength of Lewis and Brønsted acid sites were determined by a pyridine titration method. Briefly, the samples were first degassed at 450 °C for 1 hour and exposed to pyridine vapor for 1 hour followed by heating at 150 °C in He gas stream to remove physisorbed pyridine. For the temperature dependent desorption studies, the catalysts were further treated at 200 – 350 °C to desorb pyridine molecules adsorbed on

Brønsted and Lewis acid sites. Then, the catalysts were pressed to produce self-supporting wafers. Infrared spectra of the samples were collected using a Fourier transform infrared (FT-IR) spectrometer (Nicolet Nexus-670) equipped with Mercury-Cadmium-Telluride (MCT) detector at room temperature with 80 scans and 2 cm^{-1} resolution for each spectrum. Finally, the concentration of Brønsted and Lewis acid sites was determined using a molar extinction coefficient (1.13 cm/μmole for Brønsted sites and 1.28 cm/μmole for Lewis sites) of the pyridine IR band at 1540 $cm^{-1}$and 1450 cm^{-1}, respectively.[25]

Catalytic reaction studies

Gas phase n-hexadecane hydroisomerization were carried out on the catalysts described above. A tubular fixed-bed flow reactor was used for all catalytic studies at ~1 bar and 300 – 400 ºC. A stainless steel reactor tube with ¼ inch diameter was loaded with 50 – 600 mg of catalyst, whose ends were capped with a purified thermal silica paper. The remaining space in the reactor tube was filled with purified fused alumina granulate and the ends of the tube were capped with glass wool.

Before the actual reaction studies, the catalysts were pretreated at 360 ºC for 2 hours under a gas mixture of H_2 (Praxair, 5.0 UHP, 10 sccm) and N_2 (Praxair, 5.0 UHP, 10 sccm) with a heating rate of 2 ºC/min. After the pretreatment, the gas flow was changed to 16 sccm H_2 and n-hexadecane (Sigma-Aldrich, ≥99.0% purity) was introduced using a liquid flow pump (Teledyne ISCO 500D) at a rate of 0.6 mL/hour. In the reactor head, n-hexadecane was evaporated and mixed with H_2 gas to give a two-component gas flow. A Baratron type manometer (890B, MKS Instruments) was used to monitor the reactor head pressure. At the reactor outlet, the flow lines were maintained at 300 ºC to enable vapor phase sampling of the reaction products. An in-line gas chromatography-mass spectrometry (GC-MS, HP 6890 Series) equipped with an Aldrich HP-1 capillary column, a flame ionization detector (FID), and a quadrupole mass selective detector (MSD) was used to analyze the product composition. A GC-MS Chemstation software (HP) was used for automatic sampling, data collection, and post-run processing. For all catalysts, the data were collected with 1 hour of reaction time, in which no detectable catalyst deactivation was observed. Isomer selectivity, conversion, and isomer yield were calculated using the following equations:

$$\text{selectivity (\%)} = \frac{\text{the amount of isomer formed}}{\text{the amount of } n\text{-hexadecane consumed}} \times 100$$

$$\text{conversion } (\%) = \frac{\text{the amount of } n\text{-hexadecane consumed}}{\text{the amount of } n\text{-hexadecane in}} \times 100$$

$$\text{yield } (\%) = \frac{\text{the amount of isomer formed}}{\text{the amount of } n\text{-hexadecane in}} \times 100$$

RESULTS AND DISCUSSION

Aluminum modified mesoporous silica vs mesoporous zeolites

Platinum nanoparticles supported on aluminum modified mesoporous silica catalyzed gas phase n-hexadecane isomerization with remarkable selectivity (~100%). The catalytic performance of the silica based hydroisomerization catalyst was tested against the performance of zeolite catalysts commonly used for hydroconversion reactions. For all catalysts, including zeolites, synthesis parameters were carefully controlled to produce relatively high external surface area and large mesopores needed to support platinum nanoparticles. For the synthesis of silica hydroisomerization catalyst, first, amorphous silica with high surface area and large mesopore size (MCF-17, Table 1) was post-synthetically modified with aluminum to generate acidic sites essential for isomerization of linear alkanes. Then, platinum nanoparticles with 1.5 nm particle size and narrow size distribution (Figure S5), were percolated in the aluminum modified mesoporous silica to produce bifunctional catalyst with intimate metal hydrogenation/dehydrogenation and acidic sites (Pt/Al-MCF-17). Similarly, platinum nanoparticles were supported on zeolites with BEA and MFI microstructure specifically synthesized to contain comparable surface area and large mesopores (Table 1). As presented in Figure 1, Pt/Al-MCF-17 produced mainly monobranched hexadecane isomers, whereas zeolite catalysts (Pt/BEA and Pt/MFI) predominantly cracked the alkane at comparable reaction conditions.

Table 1. Physicochemical properties of aluminum modified silica and zeolite catalysts

Catalyst	Surface area (m^2/g)	Mesopore volume (cm^3/g)	Micropore volume (cm^3/g)	Si/Al mole ratio[a]	Total Al[a] (mmole/g)	Total Brønsted acid[b] (mmole/g)	Total Pt[a] (w.t. %)
Pt/Al-MCF-17	712	2.805	N/A	14.0 ± 0.2	1.15 ± 0.02	0.34	0.52 ± 0.06
Pt/BEA	630	0.790	0.109	8.0 ± 0.1	1.97 ± 0.02	1.12	0.42 ± 0.05
Pt/MFI	610	0.512	0.107	36 ± 0.2	0.32 ± 0.01	0.13	0.47 ± 0.02

[a]Determined from elemental analysis (ICP-AES, Microanalytical Lab, University of California – Berkeley)
[b]The number of total Brønsted acid sites determined by pyridine titration

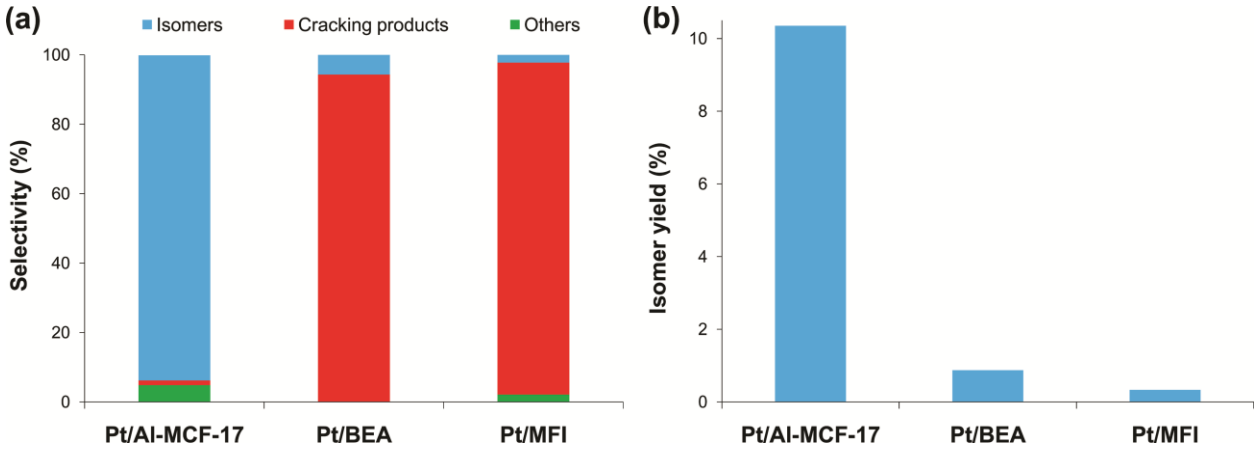

Figure 1. (a) Product selectivity and (b) isomer yield for gas phase hydroisomerization of n-hexadecane were compared for mesoporous silica and zeolite catalysts (Pt/Al-MCF-17, Pt/BEA, and Pt/MFI). The reaction was carried out at comparable conversions (10 – 15%) at 300 ºC and ~1 bar.

In hydroisomerization and hydrocracking reactions, Brønsted acid sites determine reaction rate and selectivity. Accordingly, the acidic sites of Al-MCF-17 as well as BEA and MFI zeolites were characterized with pyridine adsorption/desorption studies. Through the use of FT-IR spectroscopy, the amount of pyridine adsorbed on the acidic sites was quantified and correlated to Brønsted and Lewis acid sites (Figure S2).[26] The relative strengths of the acidic sites were characterized by desorbing the pyridine molecule as a function of temperature. As shown in Figure 2, the amount of pyridine adsorbed on Brønsted acid sites of Al-MCF-17 rapidly decreased as temperature increased. In contrast, MFI lost negligible amount of adsorbed pyridine at the temperature range studied, indicating that Brønsted acid sites of MFI zeolite are much stronger than Brønsted acid sites of Al-MCF-17 and BEA. The strength of Lewis acid sites of the catalyst was similarly characterized with temperature dependent pyridine desorption studies (Figure S3). These findings agree well with what Ryoo and coworkers determined for aluminum modified MCM-41 and MFI zeolite using ^{31}P-NMR.[27]

Significant difference in isomer selectivity observed for silica and zeolite catalysts is presumably due to difference in the strength as well as the density of Brønsted acid sites.[16, 22] It is generally accepted that hydroisomerization and hydrocracking of alkanes proceed via an alkene intermediate that is formed through a dehydrogenation step on the metal site.[28] The unsaturated intermediate then undergoes protonation and rearrangement at the Brønsted acid sites, followed by rapid hydrogenation to isoalkane. However, if the strength and density of Brønsted acid sites in zeolitic micropores are sufficiently high, alkene intermediates can undergo cracking due to

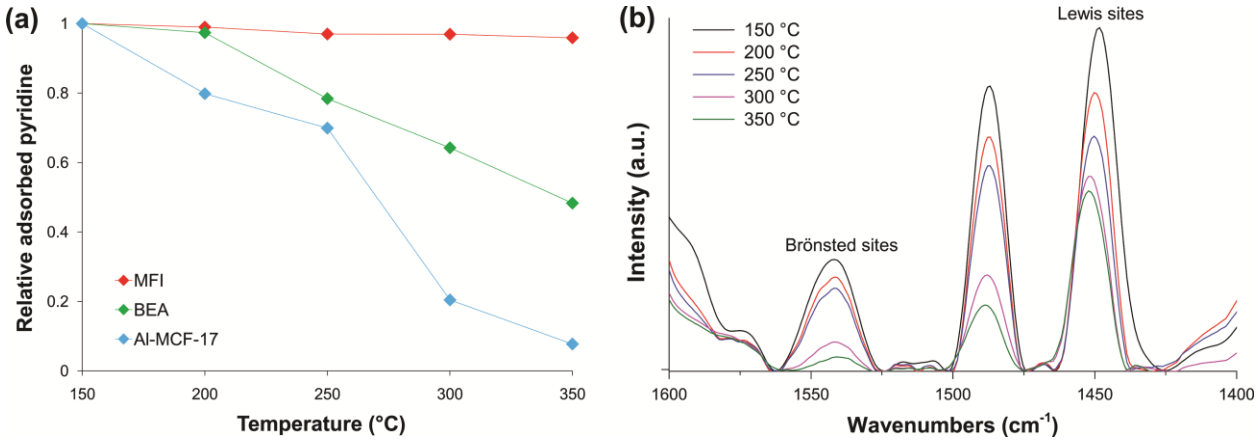

Figure 2. (a) Plots presenting temperature dependent desorption rate of pyridine molecules adsorbed on Brønsted acidic sites of MFI and BEA zeolites and Al-MCF-17, and (b) normalized FT-IR spectra of pyridine molecules adsorbed on Brønsted acidic sites of Al-MCF-17 as a function of temperature.

increased surface residence time and probability of beta scission.[29, 30] The high selectivity observed for Pt/Al-MCF-17 is primarily due to milder acid sites generated by post-synthetic doping of amorphous silica with aluminum (Figure 2a). The Brønsted acid sites of Al-MCF-17 were sufficiently strong to facilitate the formation of carbocationic intermediates (secondary carbocation) from the dehydrogenated alkane species produced by platinum nanoparticles and rearrange them into thermodynamically more stable branched counterparts (tertiary carbocation). However, they were not strong enough to crack or further fragment the carbocation intermediates to smaller hydrocarbons. In contrast to Pt/Al-MCF-17, Pt/MFI produced mainly cracked products. The high cracking capacity of the zeolite is predominantly because of its markedly strong intrinsic Brønsted acid sites. The impact of the concentration of the acid sites on the alkane cracking should be negligible as the acid density of MFI zeolite is substantially low, even lower than the acid density of Al-MCF-17. Similarly, Pt/BEA had extremely high selectivity for cracked products. In this case, however, both the strength and density of Brønsted acid sites might be contributing to increased selectivity towards cracking. As presented in Figure 2a, BEA zeolite has Brønsted acid sites with relatively moderate strength. Accordingly, the strength of the acid sites in BEA zeolite alone is less likely to account for the observed significant difference in the selectivity between Pt/Al-MCF-17 and Pt/BEA. As characterized by pyridine adsorption studies, BEA zeolite has the highest density of Brønsted acid sites while platinum is maintained at comparable amounts (Table 1). Consequently, higher concentration of acidic sites might significantly contribute to cracking of the alkane. This is also consistent with previous studies on

the effect of ratio of platinum to Brønsted acid sites. Zeolite catalysts loaded with lower amount of platinum metal tend to crack alkane more than the zeolites containing higher amount of platinum.[21, 31] The primary cause for higher cracking rate has been demonstrated to be sufficiently long residence time of intermediate species on acidic sites. The intermediates resulting from the dehydrogenation of alkane on metallic site encounter multiple acidic sites before being hydrogenated on another metallic site increasing the probability of cracking. Finally, catalytic activity of Al-MCF-17 and BEA and MFI zeolites was tested without the presence of platinum nanoparticles to confirm the difference in the strength of acidic sites between the catalysts. Unlike BEA and MFI zeolites, Al-MCF-17 was found to be completely inactive towards n-hexadecane conversion. This is consistent with our studies demonstrating that Al-MCF-17 has milder acidic sites than BEA and MFI zeolites.

Effect of catalyst microstructure and density of acid sites

The role of catalyst microstructure and concentration of surface Brønsted acid sites on hydroconversion rate and selectivity was studied using aluminum modified silica catalyst. Post-synthetic grafting method used in this work not only allows us to control over the structure of the support, but it also enables to systematically vary the amount of surface active sites without jeopardizing the structural integrity of the catalyst. Furthermore, the strength of the acid sites was not significantly affected by the change in the amount of surface aluminum sites as demonstrated in our previous work.[16] The effect of pore size and microstructure on n-hexadecane conversion was characterized by supporting the necessary amount of 1.5 nm platinum nanoparticles on aluminum grafted microporous and mesoporous silica. The silica supports employed were Santa-Barbara amorphous (SBA-15), mesocellular siliceous foam (MCF-17), and self-pillared pentasil (SPP). SBA-15 is a mesoporous amorphous silica that has been commonly used as a support for various catalysts.[32, 33] It has hexagonally aligned channel-like pores with average pore diameter of 6.4 nm as characterized by TEM and N_2 physisorption. MCF-17 is another amorphous silica with interconnected spherical pores with average diameter of 26.5 nm.[34, 35] SPP is a crystalline silica compound with hierarchical pore structure.[36] It contains both mesopores with average pore diameter of 6.5 nm and a network of ~0.5 nm micropores with MFI microstructure. All silica supports were modified with aluminum by the same post-synthetic method described in supporting information. The amount of aluminum and Brønsted acid sites were determined by elemental analysis (ICP-AES) and pyridine titration, respectively. The physicochemical

properties of the bifunctional catalysts are summarized in Table 2 and TEM images are shown in Figure 3.

Table 2. Physicochemical properties of aluminum modified microporous and mesoporous silica catalysts

Catalyst	Surface area (m^2/g)	Mesopore volume (cm^3/g)	Micropore volume (cm^3/g)	Si/Al mole ratio[a]	Total Al[a] (mmole/g)	Total Brønsted acid[b] (mmole/g)	Total Pt[a] (w.t. %)
Pt/Al-SBA-15	971	0.762	N/A	13.4 ± 0.1	1.20 ± 0.01	0.32	0.56 ± 0.04
Pt/Al-MCF-17	712	2.805	N/A	14.0 ± 0.2	1.15 ± 0.02	0.34	0.52 ± 0.06
Pt/Al-SPP	498	0.259	0.095	10.6 ± 0.3	1.50 ± 0.04	0.37	0.43 ± 0.03

[a]Determined from elemental analysis (ICP-AES, Microanalytical Lab, University of California – Berkeley)
[b]The number of total Brønsted acid sites determined by pyridine titration

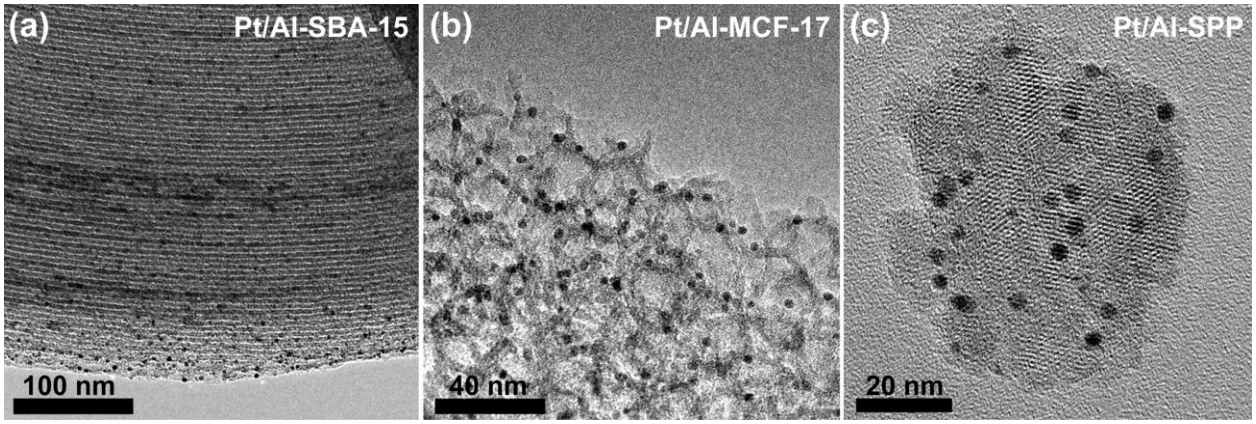

Figure 3. TEM images of hydroconversion catalysts comprising platinum nanoparticles and aluminum modified silica supports with varying pore size and structure. (a) Al-SBA-15 has ~6.4 nm wide channel-like pores aligned in hexagonal fashion. (b) Al-MCF-17 has interconnected spherical pores with ~26.5 nm diameter. (c) Al-SPP has ~6.5 nm mesopores and a network of ~0.5 nm crystalline micropores with MFI structure.

Reaction rate and selectivity was found to be highly dependent on the type of silica catalyst. The activity of each bifunctional catalyst was determined in terms of turnover frequency (TOF) calculated by normalizing the reaction rate to the number of Brønsted acid sites. According to the widely accepted mechanism for hydroisomerization or hydrocracking of alkanes,[28] dehydrogenated intermediates form on metallic site and undergo protonation and rearrangement at Brønsted acid site, followed by rapid isomerization or cracking to smaller hydrocarbons. In the presence of sufficient amount of alkene intermediates provided by the noble metal, the rate determining step is the rearrangement of the carbocation species at the Brønsted acid sites. Consequently, the rate of conversion of the reactant molecules per Brønsted acid site enables the most accurate estimation of the catalytic activity. As presented in Figure 4a, the catalysts had varying TOFs and selectivities. Aluminum modified mesoporous silica catalysts, namely Pt/Al-SBA-15 and Pt/Al-MCF-17, isomerized n-hexadecane with nearly 100%

selectivity, while Pt/Al-SPP produced considerable amount of cracked products. To elucidate the apparent difference in the hydroisomerization and hydrocracking activity presented in Figure 4a, the aluminum modified silica catalysts were further explored as a function of physicochemical surface properties. As presented in Table 2, the silica catalysts have noticeable difference in surface area and the amount of Brønsted acid sites. The most active catalyst (Pt/Al-SPP) has the lowest external surface area but the highest concentration of surface Brønsted acid sites, making its surface most densely populated with the acid sites. Likewise, the least active Pt/Al-SBA-15 has the lowest surface Brønsted acid density. In fact, regardless of the pore size and structure, hydroisomerization TOF linearly increased as a function of acid site density for the three bifunctional catalysts as shown in Figure 4b.

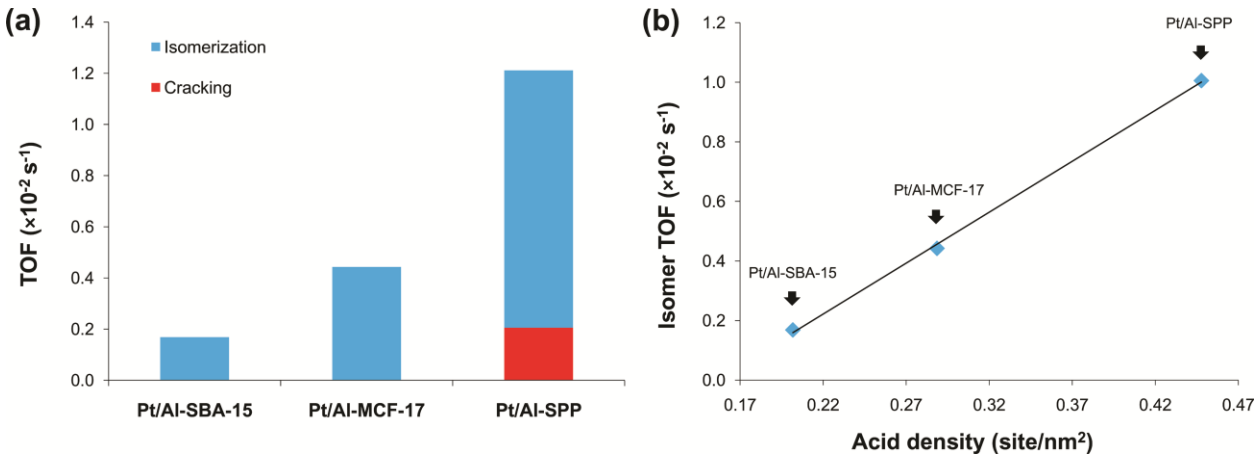

Figure 4. (a) Isomerization and cracking TOFs for n-hexadecane conversion at 300 °C as a function of aluminum modified silica catalysts with varying pore size and structure and (b) isomerization TOF as a function of surface Brønsted acid density for the aluminum modified silica catalysts. Straight line indicates linear regression applied to isomerization data points (R^2 = 0.999).

The data shown in Figure 4 is in accordance with our previous interpretation on the impact of surface Brønsted acid density on reaction selectivity. Increased number of acid sites per surface area leads to longer residence time of intermediate species on the surface. Consequently, the probability of cracking of carbocation species by beta scission mechanism increases. This phenomenon has often been observed in zeolite catalysis. For example, traditional steam calcination of zeolite catalysts increases activity and selectivity to isomerization presumably due to decreased density of aluminum sites, i.e., acid sites.[37, 38] However, it is noteworthy to mention that in zeolite catalysis systematic characterization of the change in

number and strength of acidic sites has been extremely difficult because of concomitant structural changes occurring within the zeolite.[39, 40] Nevertheless, post-synthetic aluminum doping method used in this work enables more controlled design of aluminosilicate catalysts to explore the world of acid catalysis.

Effect of platinum nanoparticle size

In addition to acid strength and density, metal loading and dispersion can significantly alter isomerization of linear alkanes on bifunctional catalysts.[16, 21, 41] Higher dispersion or more uniform inclusion of the metal nanoparticles is necessary to produce 'intimate' bifunctional sites for more efficient hydroisomerization.[42] In other words, when the distance between the acidic site and platinum site is sufficiently small, the diffusion of the reaction intermediates, such as dehydrogenated and carbocation species, does not affect the kinetics of hydroisomerization. On the contrary, larger distance might lead to decreased activity and selectivity because of increased residence time of the intermediate species and increased probability of cracking and coke formation. The 'critical' distance, beyond which catalytic activity and selectivity decreases, has often been dictated by the so-called intimacy criterion.[42, 43]

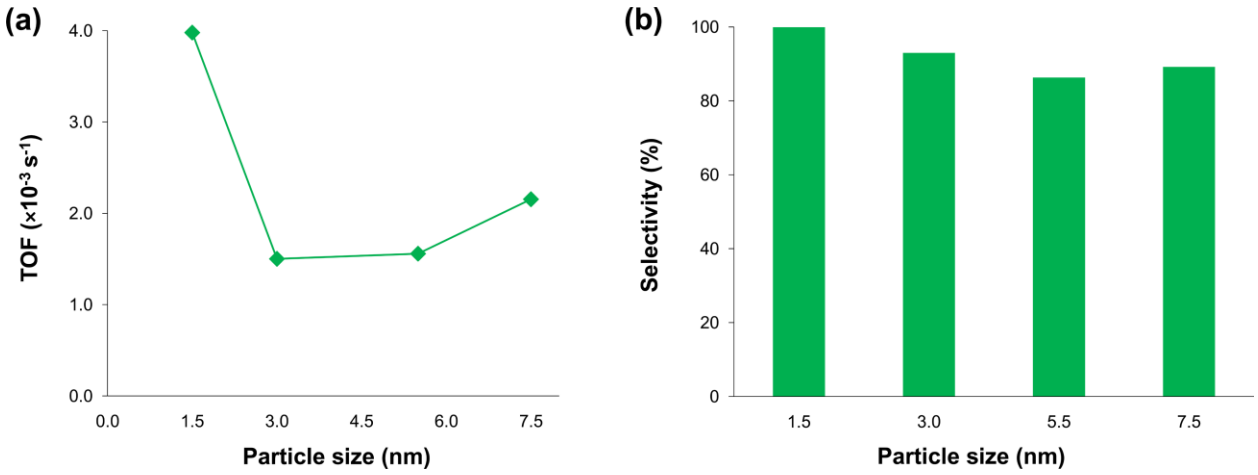

Figure 5. (a) Total TOF and (b) isomer selectivity for n-hexadecane hydroisomerization at 300 °C as a function of platinum nanoparticles size. Comparable amount of 1.5 nm, 3.0 nm, 5.5 nm, and 7.5 nm platinum nanoparticles were loaded on Al-MCF-17 by the same post-synthetic sonication method.

In this work, the flexibility of aluminum doping method allowed us to incorporate platinum nanoparticles with varying sizes in mesoporous silica with large mesopores and systematically explore the effect of platinum particle size on reaction rate and selectivity. PVP capped platinum nanoparticles with delicately controlled sizes of 1.5 nm, 3.0 nm, 5.5 nm and 7.5

nm (Figure S5) were dispersed on Al-MCF-17 which contains uniformly distributed large mesopores (Table 2, Figure 3). The TOF was calculated by normalizing the reaction rate to the number of Brønsted acid sites as they determine the rate of conversion. As presented in Figure 5, a slight dependence of the reaction rate and selectivity on platinum particle size was observed. The highest turnover rate and selectivity was achieved with 1.5 nm Pt/Al-MCF-17, exhibiting ~100% and 2.5 fold difference from the least active 3.0 nm Pt/Al-MCF-17. Furthermore, similar trend was observed in the reaction selectivity as a function of platinum particle size as shown in the figure.

The slight difference in catalytic activity and selectivity between 1.5 nm and larger platinum nanoparticles is presumably due to nonuniform incorporation of the platinum nanoparticles in the aluminum modified mesoporous silica. Even though the average pore size of MCF-17 is considerably large (~26.5 nm), the bigger platinum nanoparticles might not get fully dispersed in the mesoporous support due to relatively large particle size of the silica support (several micrometers) and smaller pore aperture of the interconnected mesopores.[34] Consequently, larger platinum nanoparticles might be primarily positioned on the outer mesopores of Al-MCF-17, producing less uniform and less 'intimate' bifunctional sites. In addition, lower number concentration of larger platinum nanoparticles (for the same mass loading) might contribute to decreased particle incorporation and decreased catalytic activity.

When the catalytic activity of the most active 1.5 nm Pt/Al-MCF-17 and the least active 3.0 nm Pt/Al-MCF-17 was compared as a function of reaction temperature increased in sequential order, the larger 3.0 nm Pt/Al-MCF-17 showed higher cracking of the alkane as well as higher deactivation rate (Figure S6). The deactivation is more likely because of coke formation as no significant sintering of platinum nanoparticles was observed (Figure S7). Lower activity and higher cracking and deactivation rate observed for the larger platinum catalysts is in line with the intimacy criterion, in which catalytic activity and selectivity of bifunctional catalyst decrease because of large distance between metal and acid sites.[43] This notion of 'the closer the better' for positioning metal and acid sites has been confirmed by numerous studies on bifunctional catalysts.[41-44] However, recent intricate study by Martens and colleagues demonstrated that closest proximity between metal and zeolite acid sites can be detrimental.[45] According to the authors, when platinum is placed inside zeolite crystals, forming the highest possible intimacy, diffusion of feed molecules and alkene intermediates decreases because of

zeolitic micropores. In other words, zeolitic micropores are the main reason for decreased selectivity. Accordingly, this effect might not be relevant to our studies, in which we use aluminum doped amorphous silica containing only large mesopores.

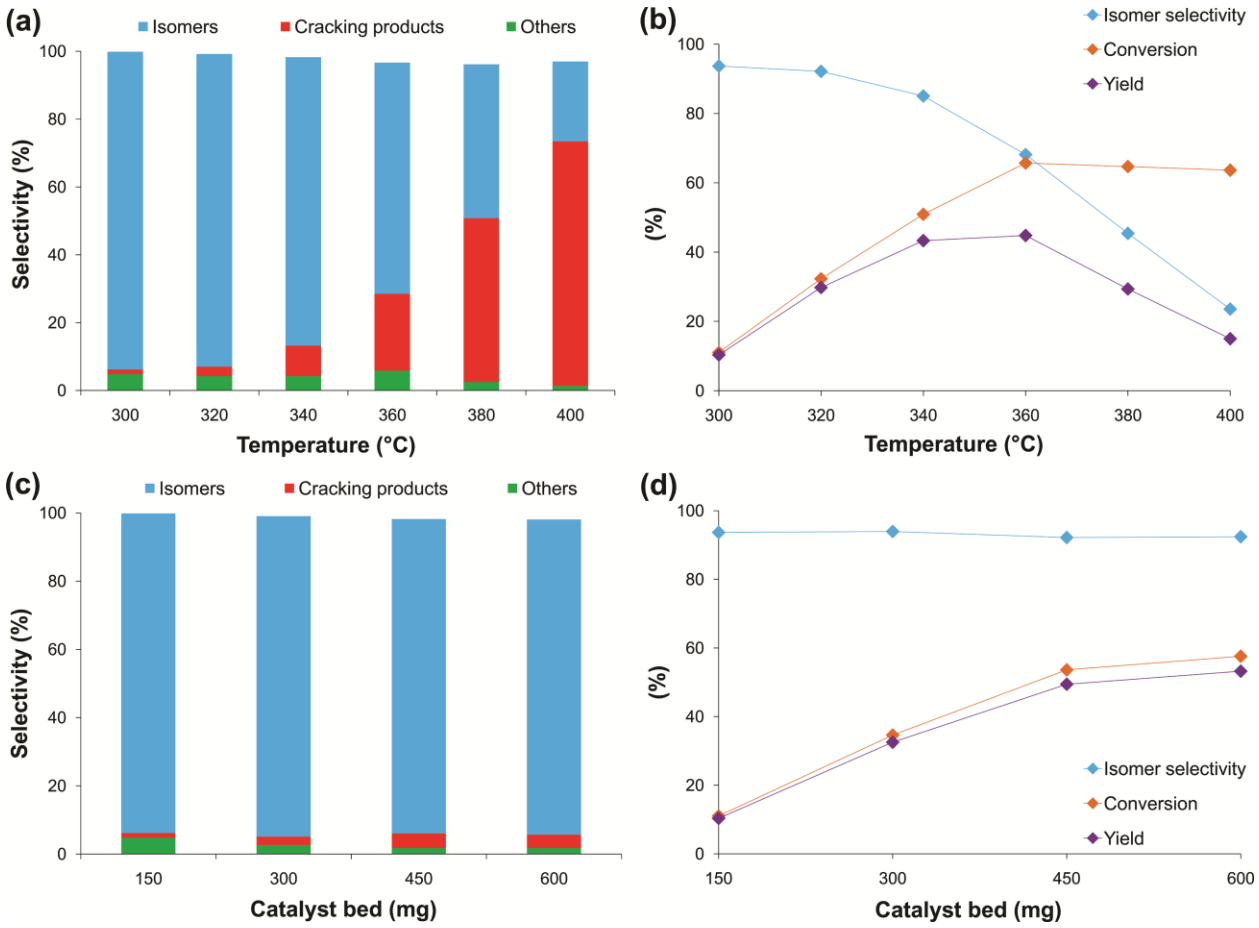

Figure 6. Overall product selectivity (a, c) and isomer selectivity, conversion, and isomer yield (b, d) as function of reaction temperature and catalyst bed, respectively. The reaction temperature was increased while keeping the catalyst bed mass constant at 150 mg (a, b), and inversely, the catalyst mass was increased while keeping the reaction temperature constant at 300 °C (c, d).

Catalytic activity of Pt/Al-MCF-17 at increased reaction conversions

Finally, the catalytic performance of the highly selective aluminum modified silica was systematically evaluated at increased reaction conversions. The total conversion was increased by increasing reaction temperature or catalyst mass. For all reaction runs, the catalytic data were collected within one hour of reaction time using fresh catalyst to avoid any catalyst deactivation and its effect on reaction conversion and selectivity. As presented in Figure 6a, at 300 °C Pt/Al-MCF-17 catalyzed n-hexadecane isomerization with considerably high selectivity. However, the

isomer selectivity consistently decreased as the reaction temperature increased, reaching less than 25% isomer selectivity at 400 °C. As the reaction reached equilibrium, the conversion maximized at 360 °C with 67%, after which no noticeable increase in conversion was observed as shown in Figure 6b. As a result, volcano shaped dependence of isomer yield on the reaction temperature was obtained. Unlike the poor selectivity obtained at high reaction temperatures, Pt/Al-MCF-17 persistently catalyzed the reaction with exceptionally high selectivity as a function of catalyst bed mass. Catalyst mass was systematically varied from 150 mg to 600 mg while keeping the reaction temperature and pressure constant at 300 °C and ~1 bar. As shown in Figures 6c and 6d, regardless of increased catalyst mass, and therefore, regardless of increased conversion, ~95% isomer selectivity was maintained at the reaction conditions tested. As a consequence, isomer yield linearly increased with increasing reaction conversion (Figure S8). Finally, it is important to mention that in industrial hydroconversion settings, high reactant conversions and pressures are more optimal because the yield for the desired products (secondary products such as highly branched isomers or cracked products) usually increases as a function of those parameters. Nevertheless, catalytic experiments run at lower reactant conversions and pressures tend to yield better mechanistic and fundamental information. This is because at these reaction conditions reactant molecules are less likely to undergo secondary reactions and the diffusion of feed molecules and intermediate species are less affected. Accordingly, in this work catalytic conversion of n-hexadecane was carried out at lower conversions and pressures for more accurate characterization of the effect of catalytically relevant factors on reaction rate and selectivity.

CONCLUSIONS

Platinum nanoparticles ‘intimately’ incorporated in aluminum modified mesoporous silica are demonstrated to catalyze isomerization of gas-phase n-hexadecane with exceptionally high selectivity, producing greater amount of isomers than platinum nanoparticles supported on mesoporous BEA and MFI zeolites. The high selectivity of the catalyst is presumably due to its sufficiently mild surface acidic sites produced by post-synthetic aluminum grafting. More importantly, the doping method allowed us to explore the effect of silica microstructure, acid site density, and platinum nanoparticle size on reaction rate and selectivity. Regardless of the pore size and structure of the aluminum modified silica support, hydroisomerization rate linearly

increases as a function of surface Brønsted acid site density. Furthermore, the catalyst with increased density of Brønsted acid sites produces higher amount of cracked products. We also find that the most active, selective, and stable catalyst is obtained with the smallest platinum nanoparticles. Consistent with intimacy criterion, the smallest nanoparticles are more likely to generate more effective bifunctional sites because of higher and more uniform inclusion in the mesoporous support with surface acid sites. Finally, we find that the high selectivity obtained with the aluminum modified silica catalyst can be retained at high reaction conversions achieved by increasing the catalyst bed mass. All in all, our work demonstrates that aluminum grafting method can be used to control product selectivity of acid catalyzed reaction by tuning surface acid sites, and therefore, surface residence time of intermediate species.

ASSOCIATED CONTENT

Supporting Information. Detailed procedure for catalyst synthesis, table summarizing physicochemical properties of the catalysts, and figures illustrating TEM images of mesoporous BEA and MFI zeolites, concentration of surface Lewis and Brønsted acid sites, average size and size distribution for platinum nanoparticles, catalytic activity and stability of 1.5 nm and 3.0 nm platinum catalysts, the change in average particle size due to sintering, and selectivity comparison for n-hexadecane and n-hexane hydroisomerization.

AUTHOR INFORMATION

Corresponding Author

*E-mail: somorjai@berkeley.edu.

Author Contributions

The manuscript was written through contributions of all authors. All authors have given approval to the final version of the manuscript.

ACKNOWLEDGMENT

We acknowledge support for this work from Chevron Energy Technology Company and the Office of Science, Office of Basic Energy Sciences, Division of Chemical Sciences, and Geological and Biosciences of the U.S. Department of Energy under contract number DE-AC02-05CH11231.

ABBREVIATIONS

Al-MCF-17, aluminum modified mesostructured cellular foam; Al-SBA-15, aluminum modified Santa Barbara amorphous; Al-SPP, aluminum modified self-pillared pentasil; MFI, mordenite framework inverted; BEA, zeolite beta polymorph A; TEM, transmission electron microscope; ICP-AES, inductively coupled plasma atomic emission spectroscopy; UHP, ultra-high purity; GC-MS, gas chromatography-mass spectrometry; FID, flame ionization detector; TOF, turnover frequency.

REFERENCES

1. R. A. Meyers, *Handbook of petroleum refining processes*, McGraw-Hill Professional, 2004.
2. A. Chica and A. Corma, *Journal of Catalysis*, 1999, **187**, 167-176.
3. R. M. Mortier, S. T. Orszulik and M. F. Fox, *Chemistry and technology of lubricants*, Springer, 1992.
4. C. Morley, *Combustion science and technology*, 1987, **55**, 115-123.
5. J. J. Kelly, C. H. Barlow, T. M. Jinguji and J. B. Callis, *Analytical Chemistry*, 1989, **61**, 313-320.
6. G. J. Antos and A. M. Aitani, *Catalytic naphtha reforming, revised and expanded*, CRC Press, 2004.
7. *US Pat.*, 4 457 832, 1984.
8. H. Weyda and E. Köhler, *Catalysis Today*, 2003, **81**, 51-55.
9. *US Pat.*, 5 980 731, 1999.
10. M. Wilson, K. Eiden, T. Mueller and S. Case, *NATIONAL PETROLEUM REFINERS ASSOCIATION-PUBLICATIONS-ALL SERIES*, 1994.
11. L. R. Rudnick and R. L. Shubkin, *Synthetic lubricants and high-performance functional fluids, revised and expanded*, CRC Press, 1999.
12. J. Scherzer and A. J. Gruia, *Hydrocracking science and technology*, CRC Press, 1996.
13. E. Iglesia, S. L. Soled and G. M. Kramer, *Journal of Catalysis*, 1993, **144**, 238-253.

14. T. Blasco, A. Chica, A. Corma, W. Murphy, J. Agúndez-Rodríguez and J. Pérez-Pariente, *Journal of Catalysis*, 2006, **242**, 153-161.
15. A. Brito, F. J. García, M. C. Alvarez-Galván, M. E. Borges, C. Díaz and V. A. de la Peña O'Shea, *Catalysis Communications*, 2007, **8**, 2081-2086.
16. N. Musselwhite, K. Na, K. Sabyrov, S. Alayoglu and G. A. Somorjai, *Journal of the American Chemical Society*, 2015, **137**, 10231-10237.
17. J. Macht, R. T. Carr and E. Iglesia, *Journal of the American Chemical Society*, 2009, **131**, 6554-6565.
18. X. Li and E. Iglesia, *Journal of Catalysis*, 2008, **255**, 134-137.
19. G. Sastre, A. Chica and A. Corma, *Journal of Catalysis*, 2000, **195**, 227-236.
20. G. E. Giannetto, G. R. Perot and M. R. Guisnet, *Industrial & Engineering Chemistry Product Research and Development*, 1986, **25**, 481-490.
21. M. Guisnet, F. Alvarez, G. Giannetto and G. Perot, *Catalysis Today*, 1987, **1**, 415-433.
22. N. Musselwhite, K. Na, S. Alayoglu and G. A. Somorjai, *Journal of the American Chemical Society*, 2014, **136**, 16661-16665.
23. C.-K. Tsung, J. N. Kuhn, W. Huang, C. Aliaga, L.-I. Hung, G. A. Somorjai and P. Yang, *Journal of the American Chemical Society*, 2009, **131**, 5816-5822.
24. Y. Borodko, H. S. Lee, S. H. Joo, Y. Zhang and G. Somorjai, *The Journal of Physical Chemistry C*, 2009, **114**, 1117-1126.
25. S. Triwahyono, A. Jalil, N. N. Ruslan, H. Setiabudi and N. Kamarudin, *Journal of Catalysis*, 2013, **303**, 50-59.
26. M. Guisnet, P. Ayrault, C. Coutanceau, M. F. Alvarez and J. Datka, *Journal of the Chemical Society, Faraday Transactions*, 1997, **93**, 1661-1665.
27. Y. Seo, K. Cho, Y. Jung and R. Ryoo, *ACS Catalysis*, 2013, **3**, 713-720.
28. G. Djéga-Mariadassou and M. Boudart, *Journal of Catalysis*, 2003, **216**, 89-97.
29. A. Corma, J. Planelles, J. Sanchez-Marin and F. Tomas, *Journal of Catalysis*, 1985, **93**, 30-37.
30. A. Corma and A. Orchillés, *Microporous and mesoporous materials*, 2000, **35**, 21-30.
31. F. Alvarez, F. R. Ribeiro, G. Perot, C. Thomazeau and M. Guisnet, *Journal of Catalysis*, 1996, **162**, 179-189.
32. R. Rioux, H. Song, J. Hoefelmeyer, P. Yang and G. Somorjai, *The Journal of Physical Chemistry B*, 2005, **109**, 2192-2202.
33. V. V. Pushkarev, K. An, S. Alayoglu, S. K. Beaumont and G. A. Somorjai, *Journal of Catalysis*, 2012, **292**, 64-72.
34. L. Wei, Y. Zhao, Y. Zhang, C. Liu, J. Hong, H. Xiong and J. Li, *Journal of Catalysis*, 2016, **340**, 205-218.
35. V. V. Pushkarev, N. Musselwhite, K. An, S. Alayoglu and G. A. Somorjai, *Nano Letters*, 2012, **12**, 5196-5201.
36. X. Zhang, D. Liu, D. Xu, S. Asahina, K. A. Cychosz, K. V. Agrawal, Y. Al Wahedi, A. Bhan, S. Al Hashimi and O. Terasaki, *Science*, 2012, **336**, 1684-1687.
37. N. Viswanadham, L. Dixit, J. K. Gupta and M. O. Garg, *Journal of Molecular Catalysis A: Chemical*, 2006, **258**, 15-21.
38. K. O. Backhaus, I. Burkhardt, H. Fichtner, U. Illgen, J. Richter-Mendau, J. Scheve and I. W. Schulz, *Applied Catalysis*, 1989, **47**, 135-144.
39. S. M. Maier, A. Jentys and J. A. Lercher, *The Journal of Physical Chemistry C*, 2011, **115**, 8005-8013.

40. L. R. Aramburo, L. Karwacki, P. Cubillas, S. Asahina, D. De Winter, M. R. Drury, I. L. Buurmans, E. Stavitski, D. Mores and M. Daturi, *Chemistry–A European Journal*, 2011, **17**, 13773-13781.
41. J. Kim, W. Kim, Y. Seo, J.-C. Kim and R. Ryoo, *Journal of Catalysis*, 2013, **301**, 187-197.
42. N. Batalha, L. Pinard, C. Bouchy, E. Guillon and M. Guisnet, *Journal of Catalysis*, 2013, **307**, 122-131.
43. P. B. Weisz, in *Advances in Catalysis*, eds. D.D. Eley, P. W. Selwood, P. B. Weisz, A. A. Balandin, J. H. De Boer, P. J. Debye, P. H. Emmett, J. Horiuti, W. Jost, G. Natta, E. K. Rideal and H. S. Taylor, Elsevier, 1962, Volume 13, 137-190.
44. J. Francis, E. Guillon, N. Bats, C. Pichon, A. Corma and L. Simon, *Applied Catalysis A: General*, 2011, **409**, 140-147.
45. J. Zecevic, G. Vanbutsele, K. P. de Jong and J. A. Martens, *Nature*, 2015, **528**, 245-248.